Structural, Electronic, Vibrational Properties and Molecular Docking of Paracetamol: a first-principle's Study

Kamalesh Khadayat[1], Bhawani Datt Joshi[1]*

[1]*Department of Physics, Siddhanath Science Campus, Tribhuvan University, Mahendranagar, 10400.*

Research Article

ISSN: 3059-9504 (online)

Article History

Received: August 8, 2024
Revised: September 6, 2024
Accepted: September 13, 2024
Published: December 28, 2024

Keywords

Paracetamol, DFT, Analgesic, Vibrational spectroscopy, Molecular Docking, MEP

***Corresponding author**

Email: bhawani.joshi@snsc.tu.edu.np
Orcid: orcid.org/0000-0003-3276-9319
Phone: +977-9841580777 (BD Joshi)
Fax: +977-99521304

ABSTRACT

Aromatic compounds are known for their biological and clinical applications. The present work explores the structural, electronic, and vibrational properties of paracetamol by DFT employing B3LYP/6-31G theory using Gaussian 09 software. To examine the equilibrium geometries, vibrational spectra, molecular electrostatic potential (MEP), lowest unoccupied molecular orbital (LUMO), highest occupied molecular orbital (HOMO), and UV-Vis spectra analysis of the tittle compound were performed. Vibrational assignments based on the potential energy distribution (PED) were made using the scaled vibrational frequencies. By using the Time Dependent DFT approach the electronic characteristics are classified. The Structure Activity Relationship has been interpreted by mapping the molecular electrostatic potential (MEP) which helps in understanding how the electronic distribution affects the molecule's behavior and interactions, particularly its activity and reactivity. Visualizing the frontier molecular orbital in both the gas and solvent phases offers important information about the reactivity, stability, as well as various structural and physical characteristics of the title compound. Additionally, the determined HOMO and LUMO energy values indicate that a charge transfer happens inside the molecule. Further, AutoDock Vina was utilized to perform the molecular docking investigation of paracetamol against the protein CYP2E1(1EQG). The docking analysis shows a -6.6 kcal/mol favorable binding affinity with the CYP2E1(1EQG) receptor, indicating a robust interaction and promising pharmacological importance.

1. NTRODUCTION

Paracetamol, also known as acetaminophen, is a widely used synthesized compound with numerous clinical applications primarily as an analgesic and antipyretic [1-3]. Since 1980s, paracetamol is the top choice for managing fever and pain in children and other demographics and it is available in both single and multiple ingredient forms [3,4]. The World Health Organization (WHO) has listed paracetamol as an essential medication [5]. Its chemical structure includes one benzene ring core with a hydroxyl group and an amide group (acetamide) attached in the para position, with a molecular formula $C_8H_9NO_2$ and a molar mass of 151.165 g/mol, and with a density of 1.293 g/ml. Its melting point is 168°C with boiling points ranging from 420°C [5,6]. The presence of lone pairs on the hydroxyl oxygen, carbonyl oxygen, and nitrogen, along with the benzene pi-cloud and the p-orbital on the carbonyl carbon, results in significant conjugation in this structure, leading to high reactivity in electrophilic aromatic substitution. Two activating groups on the benzene ring enhance electron density, causing electrophiles to preferentially react at the ortho and para positions, resulting in quicker and more specific reactions [6]. From a medical perspective, paracetamol is utilized for addressing mild to moderate pain such as headaches, colds, muscle aches, sprains, back pain, menstrual cramps, arthritis pain, and toothaches [7]. It is also prescribed to pregnant women for the management of pain and fever [8]. Unlike acetanilide and acetphenetidines, paracetamol does not cause anemia or liver damage and it is preferred over aspirin for patients prone to gastric damage or those with coagulation disorders or on anticoagulants [3]. In 2005, researchers discovered that paracetamol is metabolized in the brain by the enzyme FAAH into AM404 which enhances the endocannabinoid system and pain signal transmission, suggesting that paracetamol is a pro-drug [9]. Paracetamol is generally safe when taken at recommended dose i.e., up to 4 g per day, but prolonged use of paracetamol can lead to rare side effects such as blood abnormalities, skin rashes, and pancreatitis. In case of overdose it can cause severe complications such as sweating, nausea, vomiting, liver damage, kidney failure, severe tissue death, brain swelling, blood infection, and even death [10,11].

Literature reveals that Mallah et al. [12] described a new method using transmission FTIR spectroscopy to quickly and inexpensively measure paracetamol levels in solid pharmaceutical products. Castro-Suarez et al. [13] studied on vibrational analysis of paracetamol from commercial tablets employing ATR FTIR spectroscopy, quantum cascade laser spectroscopy, and raman spectroscopy to directly detect paracetamol in pharmaceuticals. The analysis of infrared spectra was utilized through chemometrics methods such as HQI values. Habiba et al. [14], employs spectroscopy to examine paracetamol molecules and crystals, with a specific emphasis on the structure and influence of hydrogen bonds within them. Also, Oparin et al. [15], focuses on studying paracetamol polymorphic forms through controlling external parameters at the solid sample interface using SCF technology. Wang et al. [16] conducted computational systematic examinations on paracetamol and its metabolites (AM404 and NAPQI) to investigate the fundamental mechanism of paracetamol. Many research groups have studied paracetamol's clinical activity, but structural activity, including geometry optimization, MEP, HOMO-LUMO, and molecular docking studies, remains a focus of attention. This research is focused on the structure, electronic and vibrational properties including molecular docking by using density functional theory (DFT) employing B3LYP/6-31G level of

theory. The theoretical Raman and IR spectra were examined to analyze potential energy distribution. Molecular electrostatic potential surfaces (MESP) have been generated to comprehend the connection between molecular structure and biological activity. Visualization of the HOMO-LUMO plot helps in interpreting the intramolecular charge transfer feature of the molecule. Molecular docking was conducted to examine how the title molecule binds with the proteins. Figure 1(a and b) shows the crystal and optimized molecular structure of paracetamol, respectively

.

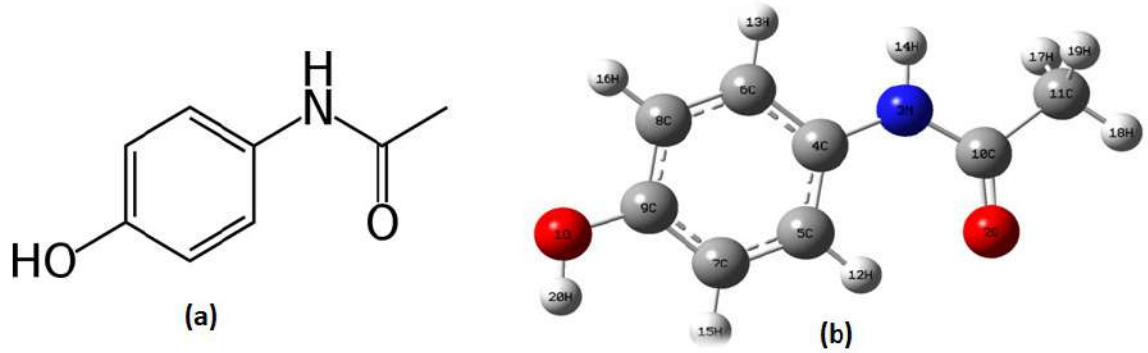

Fig. 1: (a)Molecular structure of paracetamol(Source Wikipedia) (b)Optimized geometrical structure of paracetamol.

2. MATERIALS AND METHODS

Quantum mechanical approaches are being used more frequently in computer-aidded drug design to calculate molecular orbital characteristics, dipole moments, atomic partial charges, and molecular electrostatic potential properties [17]. The initial geometry of paracetamol (PCT) was acquired from the PubChem database [18]. Using the Gaussian 09 program, the geometry was optimized employing density functional theory (DFT) at B3LYP/6-31G level without any constraints on the geometry of molecule [19] . Following geometry optimization, the vibrational frequencies of the molecule were calculated using the same level of theory. The title molecule contains 20 atoms, therefore it has 54 normal modes of vibrations based on the equation, total vibrations equal to 3N-6 [20], where N is the total number of atoms. Vibrational analysis was carried out using normal modes along with calculating potential energy distribution (PED). The calculation of potential energy distribution (PED) was done by utilizing the internal coordinates of molecular geometry with localized symmetry by Pulley's suggestion [21,22] using GAR2PED software. The Gauss-View software [23] was utilized to visually display the computed Raman and IR data. The electronic absorption wavelength was determined in solvent and gaseous phases through time-dependent density functional theory (TD-DFT) calculations [24]. AutoDock Vina [25] was used for molecular docking, while AutoDock tools [26] were utilized for preparing the ligand and protein interaction. Furthermore, Discovery Studio Visualizer was utilized for visualizing the interactions between the molecule and target protein [27].

3. RESULTS AND DISCUSSION

3.1 Geometry Optimization

The table below lists the optimal structural properties of paracetamol that were determined employing density functional theory (DFT) at B3LYP/6-31G level. It contains parameters, bond length, bond angle and dihedral angle. The number of bound electrons determines the bond length. In addition to the atoms themselves, other variables that affect the bond length between two atoms in a molecule include orbital hybridization and the electronic and steric character of the substituent. Stronger attraction between atoms and shorter bond lengths are associated with higher bond orders (number of bonded electrons).

Table 1: Optimized geometric parameters (bond length, bond angle and dihedral angles) of paracetamol.

Parameters	Bond Length (Å)	Parameters	Bond angle (˚)		Parameters angle (˚)	Dihedral
O1-C9	1.3611	C9-O1-H20	108.9008		H20-O1-C9-C7	-0.0507
O1-H20	0.9727	C4-N3-C10	128.1253		H20-O1-C9-C8	-179.973
O2-C10	1.2269	C4-N3-H14	115.2519		C10-N3-C4-C5	0.0037
N3-C4	1.3952	C10-N3-H14	116.6229		C10-N3-C4-C6	179.9847
N3-C10	1.4013	N3-C4-C5	119.9953		H4-N3-C4-C5	-179.9702
N3-H14	1.0179	N3-C4-C6	120.0026		H14-N3-C4-C6	0.0108
C4-C5	1.3948	C5-C4-C6	120.0021		C4-N3-C10-O2	0.1939
C4-C6	1.3949	C4-C5-C7	119.9939		C4-N3-C10-C11	-179.999
C5-C7	1.3949	C4-C5-H12	124.2667		H14-N3-C10-O2	-179.8325

C5-H12	1.081	C7-C5-H12	115.7394	H14-N3-C10-C11	-0.0254
C6-H13	1.087	C4-C6-H13	120.795	N3-C4-C5-H12	0.0061
C7-C9	1.3948	C8-C6-H13	119.2099	C6-C4-C5-C7	0.0142
C7-H15	1.0869	C5-C7-C9	120.0037	C6-C4-C5-H12	-179.975
C8-C9	1.3947	C5-C7-H15	119.351	N3-C4-C6-C8	-179.9858
C8-H16	1.0866	C9-C7-H15	120.6453	N3-C4-C6-H13	0.0085
C10-C11	1.5081	C6-C8-C9	120.0041	C5-C4-C6-C8	-0.0047
C11-H17	1.0936	C6-C8-H16	119.6573	C5-C4-C6-H13	179.9896
C11-H18	1.0935	C9-C8-H16	120.3386	C4-C5-C7-C9	0.0142
C11-H19	1.0937	O1-C9-C7	120.0023	C4-C5-C7-H15	-179.9862
		O1-C9-C8	119.9966	H12-C5-C7-C9	179.9759
		C7-C9-C8	120.0011	C12-C5-C7-H15	0.0038
		O2-C10-N3	127.4398	C4-C6-C8-C9	-0.0047
		O2-C10-C11	120.7964	C4-C6-C8-H16	179.9824
		N3-C10-C11	111.7635	H13-C6-C8-C9	-179.9991
		C10-C11-H17	109.74	H13-C6-C8-H16	-0.012
		C10-C11-H18	109.8233	C5-C7-C9-O1	-179.9176
		C10-C11-H19	109.8423	C5-C7-C9-C8	0.0047
		H17-C11-H18	108.9843	H15-C7-C9-O1	0.0541
		H17-C11-H19	109.5378	H15-C7-C9-C8	179.9764
		H18-C11-H19	108.893	C6-C8-C9-O1	179.9271
				C6-C8-C9-C7	0.0047
				H16-C8-C9-O1	-0.0599
				H16-C8-C9-C7	-179.9823
				O2-C10-C11-H17	118.0931
				O2-C10-C11-H18	-1.6917
				O2-C10-C11-H19	-121.4278
				N3-C10-C11-H17	-61.7287
				N3-C10-C11-H18	178.4865
				N3-C10-C11-H19	58.7504

The improved geometric characteristics of paracetamol, identified through the 6-31G basis set and DFT/B3LYP method, offer valuable information about the molecule's configuration. The bond lengths for the O1-H20 bond is 0.9727 Å. The length of a carbon-carbon bond can vary between 1.20 and 1.54 Å, contingent upon the chemical bonding type [28]. In the study , the longest C-C bond was present between C10-C11 and shortest between C8-C9 with 1.5081 Å and 1.3947 Å respectively. Significantly, the C-O bonds lengths (1.3893 Å at O1-C9 and 1.2414 Å at O2-C10) emphasize the importance of the carbonyl and hydroxyl functional groups in the molecule's pharmacological effects. In hybridization, the bond angle rises with the s character of the s hybrid bond and falls by around 2.5% as the lone pair of electrons increase. The C4-N3-C10 has the highest angle of 128.1253° indicates a planar arrangement around the nitrogen atom, which is commonly seen in amide bonds, revealing additional structural information. The angle of 119.9939° between carbons C4, C5, and C7 demonstrates the benzene ring's aromatic nature, preserving its hexagonal shape. These geometric factors highlight how the electronic and steric factors of paracetamol interact to determine its molecular shape, affecting its reactivity and its ability to bind to biological targets. Having this comprehensive structural data is crucial in comprehending how paracetamol behaves in different chemical and biological scenarios, which helps in developing pharmaceutical agents that are more efficient.

3.2 Mulliken Atomic Charges

that refers to an estimation of electron density distribution within molecules. This concept originates from Mulliken population analysis, which allocates electron density based on molecular orbital coefficients derived from quantum chemical calculations. These charges offer valuable insights into amolecule's electron distribution and partial charges, aiding in the understanding of chemical reactivity, polarity, and intermolecular interactions. However, the results can be influenced by the selected basis set and the level of theory applied in the quantum chemical calculations [29]. Mulliken charges for paracetamol are listed below in the Table 3. Carbon C10 atom with the most positive charge and is Mulliken atomic charge is a term in computational chemistry therefore expected to be the site of nucleophilic attack in the compound's title. On the other hand, nitrogen N3 has the highest negative charge and is expected to be the site for electrophilic attack. Regarding the hydrogen atoms, the majority of the Mulliken charges are concentrated at H20. Additionally, oxygen atoms are negatively charged and hydrogen atoms are positively charged. As was observed in the molecular docking section, the net negative charge on oxygen atoms (electron donor) and the positive charge on hydrogen atoms play a major role in intermolecular hydrogen bonding. The figure 2 below shows the graph of Mulliken charge against atoms.

Table 3: Mulliken Atomic Charges of paracetamol .

Label number	Symbol	Mulliken Atomic Charge	Label number	Symbol	Mulliken Atomic Charge
1	O	-0.603637	12	H	0.236887
2	O	-0.485140	13	H	0.174675
3	N	-0.831400	14	H	0.320455
4	C	0.321729	15	H	0.179464
5	C	-0.202183			
6	C	-0.204216	16	H	0.201739
7	C	-0.221731	17	H	0.215088
8	C	-0.184311	18	H	0.236429
9	C	0.280226	19	H	0.213324
10	C	0.641953	20	H	0.352767
11	C	-0.642116			

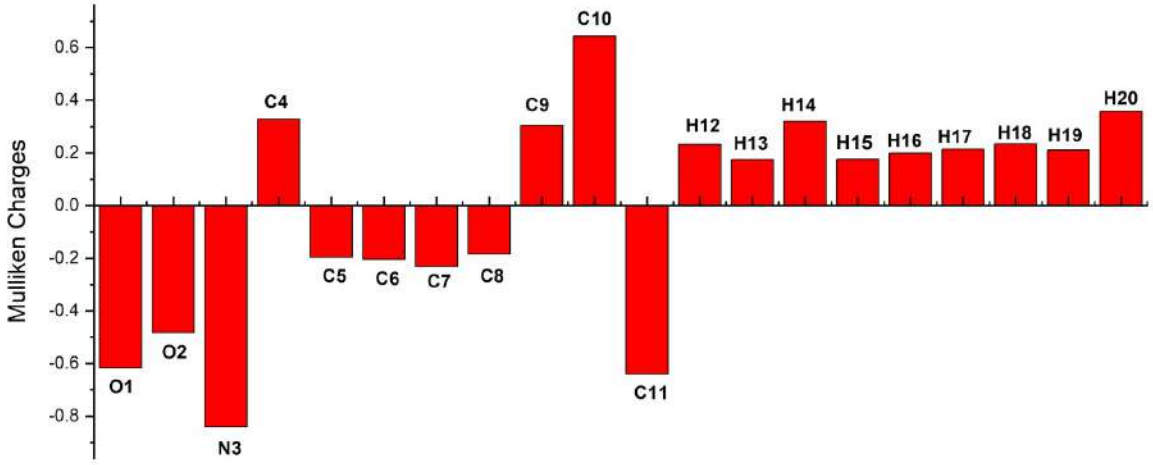

Fig. 2: Calculated Mulliken Charges of Paracetamol.

3.3 UV-Vis Spectral Analysis

The UV-Vis spectral range shows transitions between various electronic energy levels, which give rise to the absorption bands that are found there. When the frequency of incoming electromagnetic radiation coincides with the difference in energy between two electronic states, an electron is stimulated. The electronic structure of the molecule and its surroundings control the energy fluctuation. Charge dislocation and adherence to specific regulations, such as the Laporte selection rule, spin multiplicity selection rule, and coupling interaction with neighbour cations, are necessary for a transition to happen after radiation absorption [30]. TD-DFT

calculations were carried out in both the gaseous phase and a solvent (water) environment to investigate electronic transitions in terms of energies and oscillator strength. The energies, absorption wavelength, and oscillator strength of paracetamol were theoretically calculated using TD DFT, along with an examination of the chemical reactivity are represented in table 4. The calculated UV-Vis absorption spectra in solvent and gaseous phases are shown in the figures 3 and 4 respectively.

Table 4: Calculated absorption wavelength, energies and oscillator strength of paracetamol using DFT.

S.N	Transition States(Gas/Solvent)	Wavelength (nm)	Energy(eV)	Oscillator Strength	Type of transition
1	H→L+1/ H→L+1	255.28/260.79	4.8568/4.7542	0.0301/0.0415	π → π
2	H→L/ H→L	245.31/248.32	5.0541/4.9928	0.3706/0.4585	π → π
3	H-1→L/ H-2→L	243.46/235.86	5.0926/5.2567	0.0008/0.0007	π → π
4	H→L+2/ H→L+2	197.98/198.37	6.2624/6.2501	0.0361/0.0138	π → π
5	H−2→L/ H−1→L	194.84/195.99	6.3634/6.3261	0.0741/0.1304	π → π
6	H−2→L+ 1/ H−1→L+ 1	192.35/183.72	6.9020/6.7485	0.3303/0.4469	π → π
7	H−3→L+1/ H−3→L+1	177.33/179.06	6.9918/6.9242	0.0013/0.0051	π → π

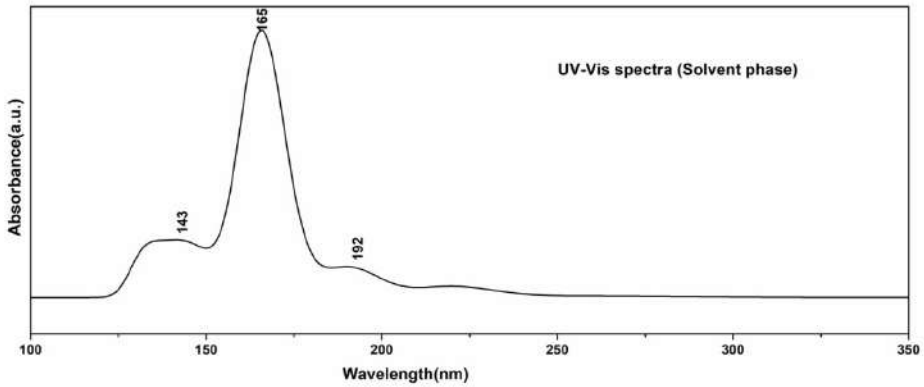

Fig. 3: UV plot of paracetamol in solvent phase between the ranges 100-350 nm.

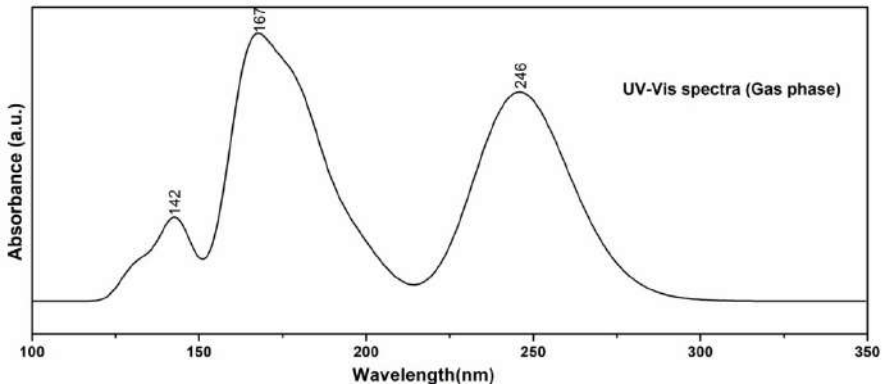

Fig. 4: UV plot of paracetamol in gas phase between the range 100-350 nm.

The prediction of electric and optical properties relies heavily on HOMO and LUMO; the bigger the energy gap, the more stable the molecules are, and vice versa. A molecule with a narrow frontier gap typically has higher conductivity and higher reactivity in chemical reactions [31], is more optically polarizable, and is kinetically less stable. The electronic transition with a high oscillatory strength (f), as well as its absorption wavelength (λ), excitation energy, and dipole moment (μ), were calculated by DFT employing B3LYP/6-31G level of theory and are shown in table 4.

The first allowed transition H→L in gas phase was calculated as 245.31nm with oscillator strength 0.3706 and in solvent phase it was at 248.32nm with oscillator strength 0.4585. The other main transitions in the gas phase were calculated at 255.28 nm (H→L+1), 243.46 nm (H-1→L), 197.98 nm (H→L+2), 194.84 nm (H–2→L), 192.35 nm (H–2→L+1) and

177.53 nm (H–3→L+1) with oscillator strengths 0.0301, 0.0008, 0.0361,0.0741, 0.3303 and 0.0013 respectively. Similarly, in the solvent phase the main transition were at 260.79 nm (H→L+1), 235.86 nm (H-2→L),198.37 nm (H→L+2), 195.99 nm (H–1→L), 183.72 nm (H–1→L+1) and 179.06 nm (H–3→L+1) with oscillator strengths 0.0415, 0.0007, 0.0138, 0.4469 and 0.0051 respectively. The mainly transition which is observed in the UV-Vis spectrum is π → π*.

Similarly, the energy difference (ΔE = E_{LUMO}–E_{HOMO}) between the two molecular orbital was 5.594 eV and 5.566 eV, respectively in the gas and solvent phases. Figure 5 shows HOMO-LUMO plot for the different molecular orbitals taking part in the charge accumulation process in the solvent and gaseous phase.

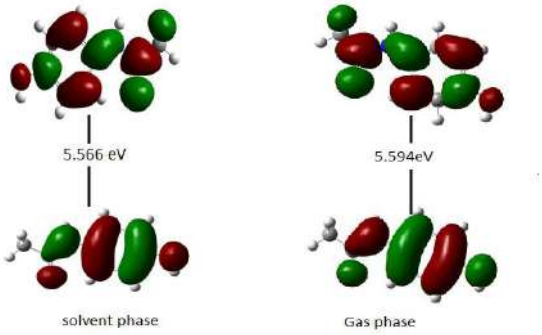

Fig. 5: HOMO-LUMO plot in gas and solvent phases.

3.4 Vibrational Assignment

The Vibrational frequency calculations were performed using the improved structural parameters to describe all of the stationary locations as minima. For every normal mode, the computed PED, IR intensity, Raman activity, and vibrational wave numbers are shown in table 5. The PED assignments were assigned using the internal coordinate system that Pulay et al. recommended. Figures 6 and 7 show the theoretically anticipated infrared and raman spectra, respectively.

Table 5: Vibrational wave numbers, Raman activity, IR intensity and Potential energy distribution [DFT/B3LYP/6- 31G] .

Wavelength		IR Intensity	Raman Activity	Potential Energy Distribution(PED)(≥5%)
unscaled	scaled			
58	58	3.560	0.594	τ(CC)(49)+τ(C10N)(15)+ρ'(C=O)(13)+[ρ(11)+ρ'(4)](CH3)[ρ(11)
77	77	0.528	1.284	[τ((43)+R[δoop(6)](C4N)+δoop(NCH)(14)+τ(C10N)(10)+R[τa](10)+R[δoop](CH)(8)
92	93	5.939	0.482	[τ(36)+R[δoop](4)](C4N)+τ(CC)(34)+R[τa](6)+ τ(C10N)(6)
165	166	9.178	0.432	γ(NCH)(36)+R[δin](C4N)(35)+ρ(C=O)(14)+ R[δin](CO)(6)
190	191	0.082	0.055	R[τa](53)+τ(C10N)(19)+τ(C4N)(6)+δoop(NCH)(6)+R[δoop](CH)(6) τ(C4N)(6)
320	321	0.778	1.579	R[δin](C4N)(25)+[δ(18)+ρ(16)](C=O)+R[δin](CO) (15)+γ(NCH)(13)
322	323	0.323	5.140	ρ(C=O)(24)+R[δa(20)+(υ(12)+δin(5))(C4N)]+ γ(NCH)(12) υ(C10N)(8)
359	360	147.646	5.271	τ(OC)(98)
399	400	5.840	2.028	R[puck](29)+R[δoop](CO)(22)+R[δoop](C4N) (18)+τ(C10N)(8)R[δoop](CH)(9)
425	425	9.235	1.715	R[δin](CO)(49)+R[δin](C4N)(19)+R[δa'](14)+δ (C=O)(9)
452	453	0.136	0.079	R[τa'](82)+R[δoop](CH)(7)
507	507	20.686	3.819	R[δa (33)+ρ'(7)](CH3)+[ρ(35)+δ(9)](C=O)
553	553	26.216	0.495	R[δoop]R[δa (CO)(31)+R[τa](30) + R[δoop](C4N)(24) + R[δoop](CH)(3)
622	622	7.216	0.920	ρ'(C=O)(58) + τ(C10N)(14)+[ρ(12)+ρ'(4)](CH3)+τ(C4N)(6)
635	633	1.405	4.147	υ(CC)(24)+R[δa]+R[δa](15)+γ(NCH)(7)+R[υ(C4N)(6) (6)+υ(CO)(6)+[δ(3)+δ(18)](C=O)](15)+γ(NCH)(7)
652	651	72.284	4.414	δoop(NCH)(53)+τ(C10N)(16)+τ(C4N)(8)+ ρ'(C=O)(6)+R[δoop](CH)(5)
680	678	0.036	6.368	R[δa'](77)
784	781	0.152	1.092	R[puck](65)+R[δoop](C4N)(17)+R[δoop](CO)(15)
804	800	16.570	21.076	υ(CO)(20)+R[δtrig](18)+υ(CC)(12)+γ(NCH)(11)+ R[υ(CC)](12)R[υ(C4N)](6)

859	854	11.865	6.248	R[δoop](CH)(86)+R[δoop](C4N)(5)+R[puck](5)
861	856	9.201	16.330	R[δa](17)+R[υ(CC)](45)+R[υ(C4N)](11)+ υ(CO)(8)+γ(NCH)(5)
895	890	97.961	0.517	R[δoop](CH)(68)+ R[δoop](C4N)(5) +R[δoop] +(CO)(13)+R[τa](11)
948	942	5.360	4.355	υ(CC)(27)+γ(NCH)(22)+[δ(22)+ υ(6)](C=O)+ υ(C10N)(10)+R[υ(CC)](5)
1002	994	0.086	2.497	R[δoop](CH)(76)+R[puck](16)
1035	1027	43.044	7.226	[[ρ'(44)+ρ(13)+δa'(3)](CH3)+υ(C10N)(16)+R[δtrig] (5)
1049	1041	0.175	0.898	R[δtrig](48)+R[υ(CC)](41)
1070	1061	5.250	1.778	R[δoop](CH)(81)+R[puck](12)
1085	1075	13.819	0.154	[[ρ](57)+[ρ'](18)+[δa(6)]](CH3)+ρ'(C=O)(15)
1149	1137	113.726	5.347	(CH)(6)+R[δin](C4N)(6)+R[υ(CC)](15)
1191	1179	199.916	7.408	δ(CHO)(34)+υ(CO)(17)+R[δin](CH)(20)+ R[υ(CC)](17)
1238	1224	3.061	24.856	R[δin](CH)(71)+R[υ(CC)](13)+R[υ(C4N)](5)
1243	1229	51.029	0.196	υ(C10N)(22)+υ(CC)(16)+R[υ(C4N)](9)+ [ρ'](CH3)(8)+R[υ(CC)](7)+[δ(9)+ρ(6)+υ(4)] (C=O)
1277	1261	150.492	40.547	R[υ(C4N)](20)+R[υ(CC)](32)+R[δtrig](11)+ R[δin](CH)(7)+υ(CO)(5)+υ(C10N)(5)+ρ](NCH)(5)
1316	1299	3.147	33.666	υ(CO)(33)+R[υ(CC)](27)+R[δin](CH)(13)+ υ(C4N)](6)
1343	1326	87.494	56.237	R[υ(CC)](59)+R[δin](CH)(8)+R[υ(C4N)](8)+υ(C10N)(6)+ δ (CHO)(5)
1396	1376	55.570	1.565	R[δin](CH)(56)+δ(CHO)(11)+R[υ(CC)](11)
1431	1411	24.853	21.476	[δs](CH3)(94)+υ(CC)(5)
1464	1442	27.238	6.096	R[δin] (CH)(35)+R[υ(CC)](26)+[ρ](NCH)(10)+δ (CHO)(7)
1526	1501	62.302	16.837	[δa'](CH3)(58)+[δa](CH3)(21)
1554	1529	11.784	28.949	[δa](CH3)(69)+[δa'](CH3)(23)+[ρ](CH3)(5)
1559	1533	403.544	40.544	R[δin](CH)(33)+R[υ(CC)](24)+[ρ](NCH)(14)+ R[υ(C4N)](9)
1581	1554	10.886	2.579	R[δin](CH)(26)+[ρ](NCH)(23)+R[υ(CC)](23)+ υ(C10N)(5)
1629	1600	28.157	15.459	R[υ(CC)](50)+[ρ](NCH)(15)+R[δa'] (7)+ R[δin](C4N)(5)
1661	1631	6.753	140.844	R[υ(CC)](56)+R[δin](CH)(21)+R[δa](11)+υ(CO)(3)
1733	1699	120.412	14.936	[υ(68)+ρ(4)](C=O)+[ρ(8)+γ(3)](NCH)+υ(C10N)(5)
3058	2932	4.232	133.539	υ(CH3)(100)
3113	2982	10.092	66.045	υ(CH3)(100)
3178	3041	4.347	72.984	R[υ(CC)](89)+υ(CH3)(10)
3181	3044	29.260	3.019	R[υ(CH)](98)
3184	3046	0.035	149.151	R[υ(CH)](97)
3234	3091	3.591	116.848	R[υ(CH)](96)
3281	3134	9.980	38.393	R[υ(CH)](99)
3524	3352	22.764	179.141	υ(OH)(100)
3540	3366	17.627	78.198	υ(NH)(99)

Proposed assignments and potential energy distribution (PED) for vibrational normal modes.
Types of vibration: ν, stretching; δ, deformation (bending); δ_{in}, in-plane bending; δ_{oop}, out-of-plane bending; ρ, rocking; τ, torsion. Potential energy distribution (contribution ≥ 5).

Vibration of Benzene ring

The frequency range of the ring carbon–carbon stretching vibrations is 1625–1430 cm^{-1} [32]. The bands exhibit variability in strength and are often observed at wavenumber of ranges 1625–1590, 1590–1575, 1540–1470, 1465–1430, and1380–1280 cm^{-1} for the five bands in the region, as provided by Varsanyi [32]. In this study, the C-C stretching vibrations were computed at 1533 and 1554 cm^{-1}. The carbon hydrogen stretching vibration give rise to bands in the region 3100 and 3000 cm^{-1} [33,34]. In this study, the virtually pure C-H stretching vibrations at a wavelength of 3044 cm^{-1} were calculated using IR intensity and Raman activity of

29.260 and 3.019 a.u, respectively. The other C-H stretching with bigger PED contributions in the scaled frequency was computed in the 3091 cm^{-1} to 3134 cm^{-1} range.

O-H Vibration

The vibrations of the hydroxyl group are expected to be the most sensitive to the environment, whether free or hydrogen-bonded. Hydrogen-bonded species cause significant variations in spectral band characteristics, including intensity, shape, and frequency location of peaks. The free hydroxyl group absorbs heavily in the 3600-3550 cm^{-1} region, but hydrogen bonds can drop the O-H stretching wavenumber to the 3550-3200 cm^{-1} area with an increase in IR intensity and breadth [35]. The study computed the pure mode (100% contribution in PED) in O-H stretching at 3352 cm^{-1}, with Raman activity and IR intensity of 179.141 and 22.764 a.u., respectively.

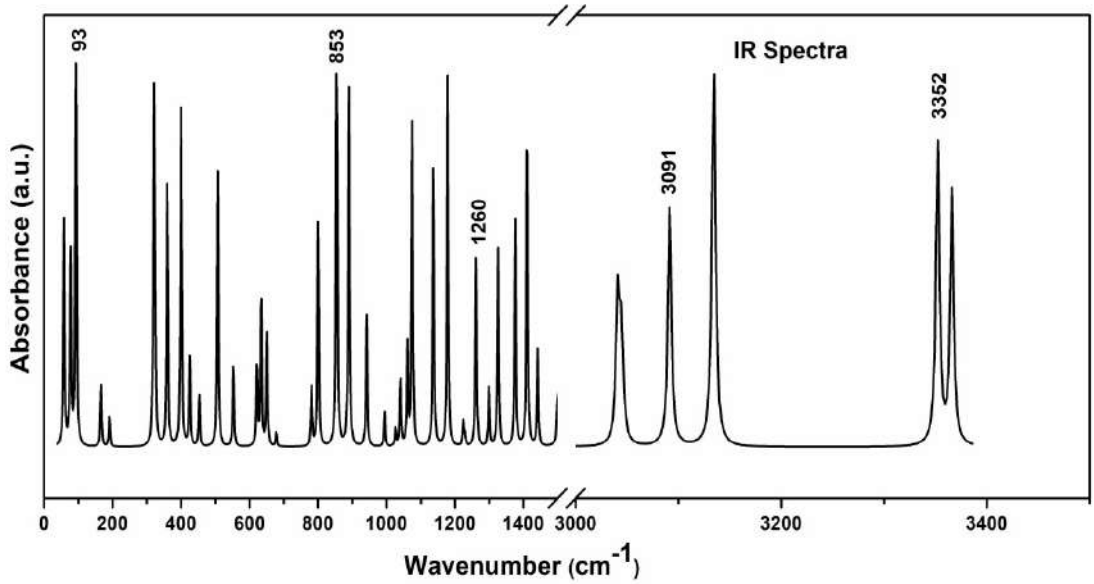

Fig. 6: IR Spectra of paracetamol between the range 0 – 3500cm^{-1} (Intensities of selected characteristics modes are assigned).

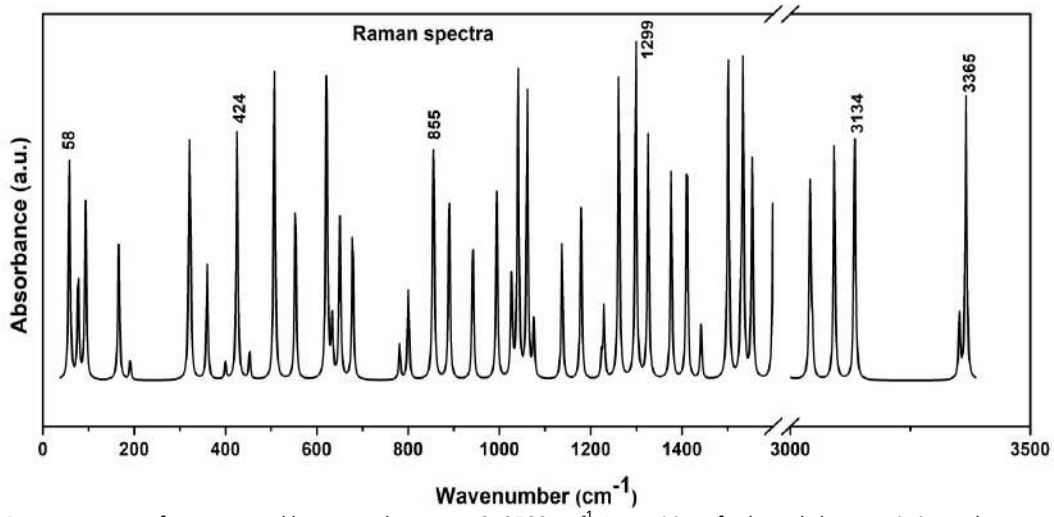

Fig. 7: Raman spectra of paracetamol between the ranges 0 -3500 cm^{-1}. Intensities of selected characteristic modes are assigned.

N-HVibration

This mode is due to the N-H bond in the amide group, which can exhibit coupling with nearby vibrations depending on the hydrogen bonding interactions. The N-H stretching absorption occurs in the range 3500-3220 cm^{-1} and is a characteristic peak that can be used to identify the presence of NH functional group in a molecule [15,36]. In this study, pure N-H stretching mode were recorded at 3366 cm^{-1} with IR intensity 17.627 and Raman intensity 78.198 respectively.

C=O Vibration

The C=O vibrations have been most widely studied by infrared spectroscopy. This multiple-bonded group is highly polar and gives rise to an intense infrared absorption band [37]. An essential spectroscopic characteristic of paracetamol is the C=O vibration, which sheds light on the molecular makeup and bonding characteristics of the substance. The C=O stretching vibration often shows in the range of 1670–1820 cm^{-1} [38]. In the present study, C=O vibration were recorded at 1699 cm^{-1} with IR intensity and Raman activity of 120.412 and 14.936

units respectively in scaled DFT.

3.5 Molecular Electrostatic Potential (MEP) surface

The MEP at a point r in the space around a molecule (in atomic units) can be expressed as [39]:

$$V(r) = \sum_A \frac{z_A}{\left|\vec{R}_A - \vec{r}\right|} - \int \frac{\rho\left(\vec{r}_1{}'\right) dr'}{\left|\vec{r}' - \vec{r}\right|}$$

where ρ (r′) is the molecule's electronic density function and Z_A is the charge on nucleus A, which is situated at R_A. The contributions of nuclei and electrons to the potential are denoted by the first and second terms, respectively. The resultant, or V(r), is the net electrostatic impact that the molecule's nuclei and electrons create at each location r. The MEP is a valuable measure for elucidating the structure–activity connection, hydrogen bonding, and reactivity of compounds, including pharmaceuticals and biomolecules [40]. The dipole moment, electronegativity, partial charges, and chemical reactivity site of a molecule are all correlated with the total chargedistribution [41]. In the MEP, the green zone denotes the neutral region, while the red and blue regions relate to the electron-rich and electron-poor regions.

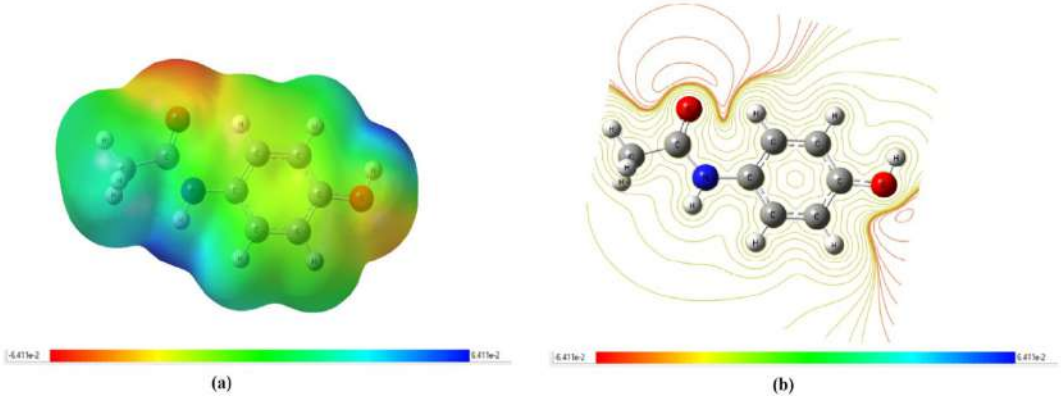

Fig. 8: (a) Molecular electrostatic potential map, and (b) Contour plot of molecular electrostatic potential surface of paracetamol.

Using the computer program GaussView, the MEP for paracetamol was plotted using the 6-31G basis set in order to estimate the reactive sites of the molecule. Figure 8 displays MEP surfaces for paracetamol. The MEP (Figure 8) for paracetamol demonstrates that the O atom of the C=O group of the molecule has a visible negative electrostatic potential surface, making it amenable to electrophilic assault. The positive charge is localised on the H atom attached to the hydroxyl group. Potential rises in red, orange, yellow, green, and blue order [42]. The proton's attraction is caused by the negative region of MEP.

3.6 Molecular Docking

Molecular docking is a potent computer method at the forefront of molecular biology and contemporary drug development. It is essential to comprehending how small molecules like possible therapeutic compounds interact with their target biomolecules, which are usually proteins or nucleic acids. Molecular docking offers important insights into the binding affinities, binding modes, and structural dynamics that control the formation of these crucial molecular complexes by emulating the binding process between these molecules in silico [43]. The protein structure for protein CYP2E1 (1EQG), which is used to dock paracetamol, was retrieved from the Protein Data Bank (PDB). In order to optimize the geometry for accurate binding simulations, the structure was cleaned by removing excess water molecules, adding any missing polar hydrogen atoms, and adjusting charge assignments and force fields. Similarly, using tools such as pyMol, the ligand paracetamol was produced in PDB format from SDF format. AutodockTools defines docking parameters and specifies PDBQT (Protein Data Bank, partial charge Q and type T) files for ligand paracetamol and receptor protein CYP2E1(1EQG). Using available literature or binding site prediction tools, the binding site on CYP2E1 (1EQG) was located. A grid box was then constructed around the binding site to provide targeted docking simulation on the active site with the highest interaction potential.

The docking simulation was carried out using programs such as AutoDock, AutoDock Vina [25,26], Glide by modifying settings including grid box dimensions 40Å× 40Å× 40Å, search strategy, and scoring function. The grid box is set at x-axis, y-axis and z-axis at 46.985, 33.471 and 187.492 directions respectively with spacing of 0.375Å. By comparing the docking scores, which indicate binding and visually inspecting significant chemical interactions such hydrogen bonding, pi-pi stacking, and hydrophobic contacts, the results were assessed to determine the optimal binding configuration for paracetamol. In order to visualize the binding interactions and significant residues, the protein-ligand complex with the top docking posture was imported into BIOVIA Discovery Studio [27] and 2D and 3D interaction maps were created. Detailed reports that highlighted the interaction details, examined the binding site structure, and assessed paracetamol's potential as a modulator of CYP2E1 (1EQG)'s function were produced using these graphics. To sum up, the outcomes were documented by keeping photos and notes for further analysis and reporting. n 1963, Ramachandran et al. presented the [phi(ϕ),psi(Ψ)] angles as a way to represent the protein backbone.

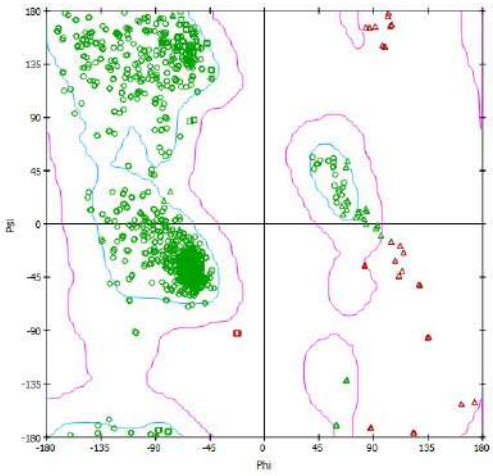

Fig. 9: Ramachandran plot of protein 1EQG.

Ramachandran plot, is widely employed in protein structure determination and secondary structure definition. Ramachandran et al. created a steric map of the Ramachandran plot based on analyzing local hard-sphere repulsions between atoms that are third neighbors (1-4 interactions), which forecasted the usual permissible regions: the α_R , α_L, and β-regions. The steric map shown in Figure 9 is now widely accepted as the typical way to interpret the Ramachandran plot, as established by Richardson in 1981. Mandel and colleagues were the first to pinpoint the precise steric clashes that establish the limits of this standard steric map [44] .The figure shows heavy residue in the alpha helix region ($\alpha_{R)}$ suggesting the significant secondary structure.

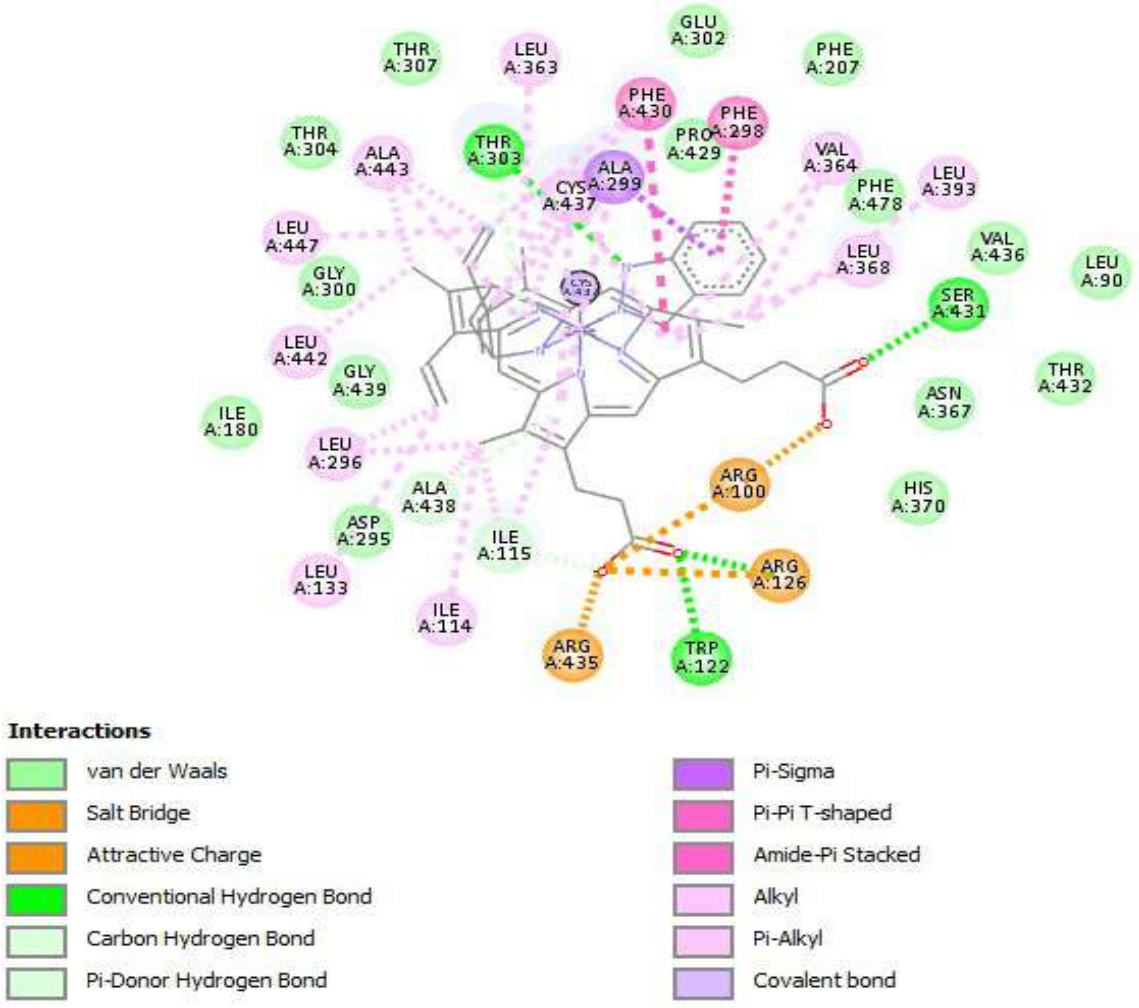

Fig. 10: 2D- ligand intraction diagram of paracetamol with CYP2E1(1EQG)

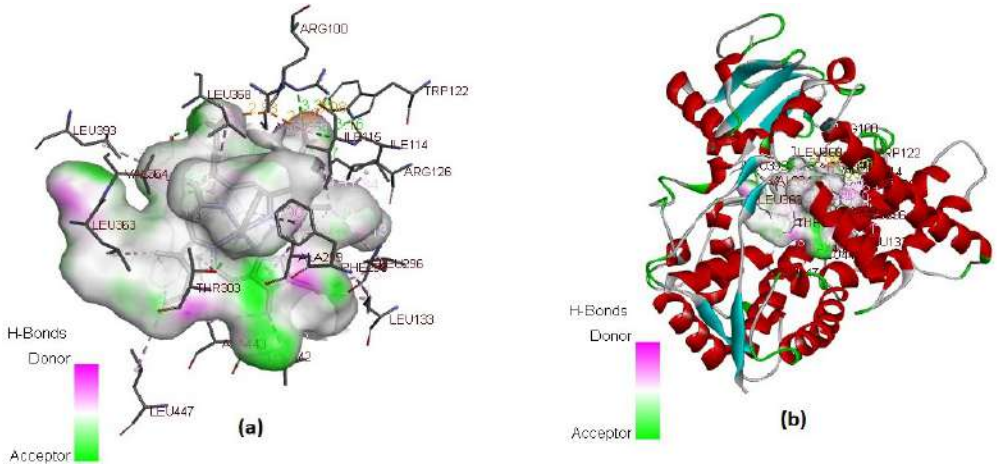

Fig. 11: (a**)** Docked structure showing binding pocket in terms of H-bond (b) Docked 3D structure showing binding pocket in terms of H-bond with receptor.

4. CONCLUSION

An analysis of the structural, electronic, and vibrational characteristics of paracetamol was carried out through DFT, alongside a molecular docking investigation with AutoDock Vina, to study the molecular structure, vibrational frequencies, MEP, HOMO-LUMO analysis, and molecular docking of the compound. It was observed that all the calculated vibrational modes were active in both IR and Raman spectroscopy. Information on the title molecule's size, shape, charge density distribution, and chemical reactivity sites has been gathered through MEP mapping. Negative potential is situated close to the O atom of the C=O group of the molecule, while positive potential is situated near the hydrogen atom of the hydroxyl group. Additionally, the pale yellow area within the benzene structure was forecasted to be a transitional phase. Using the TD-DFT/B3LYP/6-31G basis set, the electronic transition has been calculated in both the gas phase and the aqueous environment (water), illustrating the charge transfer within the molecule. The role of charge transfer between the acceptor and donor groups was made extremely evident by HOMO-LUMO. The HOMO-LUMO analysis indicated an energy gap of 5.594 eV in the gas phase and 5.566 eV in solvent, highlighting the molecule's chemical reactivity and stability. This shows that paracetamol is somewhat more reactive in a solution, which is crucial for its interaction with biological systems. Moreover, predictions have been made regarding the binding locations of the protein matrix and the title molecule. The protein CYP2E1(1EQG) molecule complex was estimated to have a binding affinity of -6.6 kcal/mol. Therefore, the title molecule has a good binding potential against the protein CYP2E1(1EQG), as theoretically demonstrated by the molecular docking studies demonstrating the significance in the fields of medicinal chemistry, title molecular chemical biology, pharmacology,and drug design in the creation of novel medications and materials. This study highlights the importance of computational chemistry in drug discovery and development, promoting its continuous use and integration in the field.

AUTOR CONTRIBUTIONS

K. Khadayat: Writing-original draft, investigation, and Formal analysis; B.D. Joshi: Methodology, Writing-review and editing, Conceptualization, and supervision

CONFLICTS OF INTEREST

There are no conflicts to declare.

ACKNOWLEDGEMENTS

B.D Joshi would like to acknowledge University Grants Commission, Nepal for partial financial support under Faculty Research Grant (FRG--79&80-S&T-05).

REFERENCES

[1] H.N. Morse, Ueber eine neue Darstellungsmethode der Acetylamidophenole, *European Journal of Inorganic Chemistry,* **11** (1878) 232-233. https://doi.org/10.1002/cber.18780110151

[2] M.J. Smilkstein, G.L. Knapp, K.W. Kulig, B.H. Rumack, Efficacy of oral N-acetylcysteine in the treatment of acetaminophen overdose: analysis of the national multicenter study (1976 to 1985), *The New England Journal of Medicine,* **319** (1988) 1557–1562. https://doi.org/10.1056/NEJM198812153192401

[3] A. Bertolini, A. Ferrari, A. Ottani, S. Guerzoni, R. Tacchi, S. Leone, Paracetamol: New vistas of an old drug, *CNS Drug Reviews,* **12** (2006) 250–275. https://doi.org/10.1111/j.1527-3458.2006.00250.x

[4] L.O. Ahmed, R.A. Omer, Computational study on paracetamol drug, *Journal of Physical Chemistry and Functional Materials,* **3** (2020) 9-13.

[5] O.O. Oloyede, Z.O. Alabi, A.O. Akinyemi, S.F. Oyelere, B.O. Amuwaolorun, B.C.D. Owoyemi, Comparative evaluation of acetaminophen form (I) in commercialized paracetamol brands, *Scientific African,* **19** (2023) e01537. https://doi.org/10.1016/j.sciaf.2022.e01537

[6] U. Freo, C. Ruocco, A. Valerio, I. Scagnol, E. Nisoli, Paracetamol: A review of guideline recommendations, *Journal of Clinical Medicine,* **10** (2021) 3420. https://doi.org/10.3390/jcm10153420

[7] O. Airaksinen, J.I. Brox, C. Cedraschi, J. Hildebrandt, J. Klaber-Moffett, F. Kovacs, A.F. Mannion, S. Reis, J.B. Staal, H. Ursin, G. Zanoli, European guidelines for the management of chronic nonspecific low back pain, *European Spine Journal,* **15** (2006) S192–S300.

https://doi.org/10.1007/s00586-006-1072-1

[8] A. Lupattelli, O. Spigset, M.J. Twigg, K. Zagorodnikova, A.C. Mårdby, M.E. Moretti, M. Drozd, A. Panchaud, K. Hämeen-Anttila, A. Rieutord, R.G. Juraski, M. Odalovic, D. Kennedy, G. Rudolf, H. Juch, A. Passier, I. Björnsdóttir, H. Nordeng, Medication use in pregnancy: A cross-sectional, multinational web-based study, *BMJ Open,* **4** (2014) e004365. https://doi.org/10.1136/bmjopen-2013-004365

[9] E.D. Hogestatt, B.A.G. Jönsson, A. Ermund, et al., Conversion of acetaminophen to the bioactive N-acylphenolamine AM404 via fatty acid amide hydrolase-dependent arachidonic acid conjugation in the nervous system, *Journal of Biological Chemistry,* **280** (2005) 31405–31412. https://doi.org/10.1074/jbc.M501489200

[10] J.L. Finnan, R.E. Lisa, D.N. Schmidt, Process for preparing spray dried acetaminophen powder and the powder prepared thereby, (U.S. Patent No. 4,710,519), *U.S. Patent and Trademark Office,* http://www.t3db.ca/toxins/t3d2571, 1975.

[11] S.Shiffman, D.R. Battista, J.P. Kelly, M.K. Malone, R.B. Weinstein, D.W. Kaufman, Prevalence of exceeding maximum daily dose of paracetamol, and seasonal variations in cold-flu season, *British Journal of Clinical Pharmacology,* **84** (2018) 1250–1257. https://doi.org/10.1111/bcp.13551

[12] M.A. Mallah, S.T. Sherazi, M.I. Bhanger, S.A. Mahesar, M.A. Bajeer, A rapid Fourier-transform infrared (FTIR) spectroscopic method for direct quantification of paracetamol content in solid pharmaceutical formulations, *Spectrochimica Acta Part A: Molecular and Biomolecular Spectroscopy,* **141** (2015) 64–70. https://doi.org/10.1016/j.saa.2015.01.036J.

[13] R. Castro-Suarez, M. Vásquez-Osorio, S.P. Hernandez-Rivera, A.A. Pájaro-Payares, Vibrational analysis of acetaminophen from commercial tablets, *IOP Conference Series: Materials Science and Engineering,* **519** (2019) 012006. https://doi.org/10.1088/1757-899X/519/1/012006

[14] U. Habiba, A. Alam, S.U.D. Rahman, S. Piya, IR spectra of paracetamol, *Bangladesh Journal of Scientific and Industrial Research,* **56** (2021) 255-262. https://doi.org/10.3329/bjsir.v56i4.57197

[15] R.D. Oparin, M. Moreau, I. De Walle, M. Paolantoni, A. Idrissi, M.G. Kiselev, The interplay between the paracetamol polymorphism and its molecular structures dissolved in supercritical CO2 in contact with the solid phase: In situ vibration spectroscopy and molecular dynamics simulation analysis, *European Journal of Pharmaceutical Sciences,* **77** (2015) 48–59. https://doi.org/10.1016/j.ejps.2015.05.016

[16] Y. Wang, W. Lin, N. Wu, X. He, J. Wang, Z. Feng, X.-Q. Xie, An insight into paracetamol and its metabolites using molecular docking and molecular dynamics simulation, *Journal of Molecular Modeling,* **24** (2018) 243. https://doi.org/10.1007/s00894-018-3790-9

[17] M.P. Gleeson, D. Gleeson, QM/MM calculations in drug discovery: A useful method for studying binding phenomena? *Journal of Chemical Information and Modeling,* **49** (2009) 670–677. https://doi.org/10.1021/ci800419j

[18] H.E. Pence, A. Williams, ChemSpider: an online chemical information resource, *Journal of Chemical Education,* **87** (2010) 1123–1124. https://doi.org/10.1021/ed100697w

[19] C. Lee, W. Yang, R.G. Parr, Development of the Colle-Salvetti correlation-energy formula into a functional of the electron density, *Physical Review B,* **37** (1988) 785–789.https://doi.org/10.1103/PhysRevB.37.785R

[20] Mishra, B.D. Joshi, A. Srivastava, P. Tandon, S. Jain, Quantum chemical and experimental studies on the structure and vibrational spectra of an alkaloid—Corlumine, *Spectrochimica Acta Part A: Molecular and Biomolecular Spectroscopy,* **118** (2014) 470–480. https://doi.org/10.1016/j.saa.2013.09.015

[21] P. Pulay, G. Fogarasi, F. Pang, J.E. Boggs, Systematic ab initio gradient calculation of molecular geometries, force constants, and dipole moment derivatives, *Journal of the American Chemical Society,* **101** (1979) 2550-2560. https://doi.org/10.1021/ja00504a009

[22] G. Fogarasi, X. Zhou, P.W. Taylor, P. Pulay, The calculation of ab initio molecular geometries: Efficient optimization by natural internal coordinates and empirical correction by offset forces, *Journal of the American Chemical Society,* **114** (1992) 8191-8201. https://doi.org/10.1021/ja00047a032

[23] A. Frisch, A.B. Nielson, A.J. Holder, *GaussView User Manual,* Gaussian Inc., Pittsburgh, P.A. https://www.scirp.org/reference/referencespapers? Reference id :1525346,2000.

[24] M.E. Casida, K.C. Casida, D.R. Salahub, Excited-state potential energy curves from time-dependent density-functional theory: A cross section of formaldehyde's 1 A1 manifold, *International Journal of Quantum Chemistry,* **70** (1998) 933–941. https://doi.org/10.1002/(SICI)1097-461X(1998)70:4/5<933::AID-QUA39>3.0.CO;2-Z

[25] O Trott, A.J. Olson, AutoDock Vina: improving the speed and accuracy of docking with a new scoring function, efficient optimization, and multithreading, *Journal of Computational Chemistry,* **31** (2010) 455–461. https://doi.org/10.1002/jcc.21334

[26] G.M. Morris, R. Huey, W. Lindstrom, M.F. Sanner, R.K. Belew, D.S. Goodsell, A.J. Olson, AutoDock4 and AutoDockTools4: Automated docking with selective receptor flexibility, *Journal of Computational Chemistry*, **30** (2009) 2785–2791. https://doi.org/10.1002/jcc.21256.

[27] Dassault Systèmes, BIOVIA Discovery Studio, Dassault Systèmes, https://www.3ds.com/products/biovia/discovery-studio, 2016.

[28] C. Corminboeuf, F. Tran, J. Weber, The role of density functional theory in chemistry: Some historical landmarks and applications to zeolites, *Journal of Molecular Structure: THEOCHEM*, **762** (2006) 1–7. https://doi.org/10.1016/j.theochem.2005.07.03.

[29] R.S. Mulliken, Electronic Population Analysis on LCAO–MO Molecular Wave Functions. I, *The Journal of Chemical Physics*, **23** (1955) 1833–1840. https://doi.org/10.1063/1.1740588.

[30] M. Picollo, M. Aceto, T. Vitorino, UV-Vis spectroscopy, *Physical Sciences Reviews*, **08** (2018) 1-14. https://doi.org/10.1515/psr-2018-0008.

[31] D. Lewis, C. Ioannides, D. Parke, Interaction of a series of nitriles with the alcohol-inducible isoform of P450:

Computer analysis of structure—activity relationships, *Xenobiotica*, **24** (1994) 401–408. https://doi.org/10.3109/00498259409043243.

[32] G. Varsanyi, Assignments for Vibrational Spectra of Seven Hundred Benzene Derivatives, Wiley, New York, 1974.

[33] V.K. Rastogi, M. Alcolea Palafox, R.P. Tanwar, L. Mittal, 3,5-Difluorobenzonitrile: ab initio calculations, FTIR and Raman spectra, *Spectrochimica Acta Part A: Molecular and Biomolecular Spectroscopy*, **58** (2002) 1987–2004. https://doi.org/10.1016/s1386-1425(01)00650-3.

[34] M. Karaback, et al., An experimental and theoretical study of molecular structure and vibrational spectra of 2-chloronicotinic acid by density functional theory and ab initio Hartree-Fock calculations, *Journal of Molecular Structure*, **885** (2008) 28–35. https://doi.org/10.1016/j.molstruc.2007.10.004.

[35] N.B. Clothup, L.H. Daly, S.E. Wiberley, Introduction to infrared and Raman spectroscopy, Academic Press, 1990.

[36] B.D. Joshi, G. Thakur, M.K. Chaudhary, Molecular Structure, Homo-Lumo and Vibrational Analysis of Ergoline by Density Functional Theory, *Scientific World*, **14** (2021) 21–30. https://doi.org/10.3126/sw.v14i14.34978.

[37] G. Socrates, Infrared and Raman Characteristic Group Frequencies, Tables and Charts, 3rd ed., Wiley, Chichester, 2001.

[38] A. Prabakaran, S. Muthu, Normal Coordinate Analysis and Vibrational Spectroscopy (FT-IR and FT-Raman) Studies of (2S)-2-Amino-3-(3,4- Dihydroxyphenyl)-2-ethylpropnoic Acid Using ab Initio HF and DFT Method, *Spectrochim. Acta Part A*: *Molecular and Biomolecular Spectroscopy*, **99** (2012) 90–96. https://doi.org/10.1016/j.saa.2012.09.014

[39] R. Parthasarathi, J. Padmanabhan, U. Sarkar, et al., Toxicity analysis of benzidine through chemical reactivity and selectivity profiles: A DFT approach, *Internet Electronic Journal of Molecular Design*, **2** (2003) 798–813.

[40] S. Chidangil, P. Mishra, Structure-activity relationship for some 2',3'-dideoxynucleoside anti-HIV drugs using molecular electrostatic potential mapping, *Journal of Molecular Medicine*, **3** (1997) 172–181. https://doi.org/10.1007/s008940050029.

[41] B.D. Joshi, P.N. Chaudhary, Molecular structure, MESP, HOMO-LUMO, and vibrational analysis of β-Asarone using density functional theory, *Kathmandu University Journal of Science, Engineering and Technology*, **9** (2013) 1–14. https://doi.org/10.3126/kuset.v9i2.63714.

[42] J.B. Khadka, B.D. Joshi, Molecular electrostatic potential, HOMO-LUMO and vibrational study of aristolochic acid II using density functional theory, *BIBECHANA*, **12** (2014). https://doi.org/10.3126/bibechana.v12i0.11702.

[43] B. Jacobs, P. Ir, M. Bigdeli, P.L. Annear, W. Van Damme, Addressing access barriers to health services: An analytical framework for selecting appropriate interventions in low-income Asian countries, *Health Policy and Planning*, **27** (2012) 288–300. https://doi.org/10.1093/heapol/czr038.

[44] B.K. Ho, A. Thomas, R. Brasseur, Revisiting the Ramachandran plot: Hard-sphere repulsion, electrostatics, and H-bonding in the α-helix, *Protein Science*, **12** (2009) 2508–2522. https://doi.org/10.1110/ps.03235203